AID-deficient Bcl-xL transgenic mice develop delayed atypical plasma cell tumors with unusual Ig/Myc chromosomal rearrangements

Alexander L. Kovalchuk,[1,4] Wendy duBois,[1] Elizabeth Mushinski,[1] Nicole E. McNeil,[2] Carsten Hirt,[1,3] Chen-Feng Qi,[4] Zhaoyang Li,[4] Siegfried Janz,[1,5] Tasuku Honjo,[6] Masamichi Muramatsu,[7] Thomas Ried,[2] Timothy Behrens,[8] and Michael Potter[1]

[1]Laboratory of Cancer Biology and Genetics, [2]Genetics Branch, Cancer Genomics Section, National Cancer Institute (NCI), National Institutes of Health, Bethesda, MD 20892
[3]Ernst-Moritz-Arndt University, D-17487 Greifswald, Germany
[4]Laboratory of Immunopathology, National Institute of Allergy and Infectious Diseases, National Institutes of Health, Rockville, MD 20852
[5]Department of Pathology, University of Iowa, Carver Roy J. and Lucille A. Carver College of Medicine, Iowa City, IA 52242
[6]Department of Immunology and Genomic Medicine, Kyoto University, Graduate School of Medicine, Kyoto 606-8501, Japan
[7]Department of Molecular Genetics, Graduate School of Medical Science, Kanazawa University, Kanazawa 920-8640, Japan
[8]Genentech, Inc., South San Francisco, CA 94080

Activation-induced cytidine deaminase (AID) is required for *immunoglobulin* (*Ig*) class switch recombination and somatic hypermutation, and has also been implicated in translocations between *Ig* switch regions and *c-Myc* in plasma cell tumors in mice. We asked if AID is required for accelerated tumor development in pristane-treated Bcl-xL transgenic BALB/c mice deficient in AID (pBx*Aicda*–/–). pBx*Aicda*$^{-/-}$ mice developed tumors with a lower frequency (24 vs. 62%) and a longer mean latency (108 vs. 36 d) than AID-sufficient mice. The tumors appeared in oil granuloma tissue and did not form ascites. By interphase fluorescence in situ hybridization, six out of nine pBx*Aicda*$^{-/-}$ primary tumors had T(12;15) and one had T(6;15) chromosomal translocations. Two tumors were transplantable and established as stable cell lines. Molecular and cytogenetic analyses showed that one had an unusual unbalanced T(12;15) translocation, with *IgH* Cμ and *Pvt-1* oriented head to tail at the breakpoint, resulting in an elevated expression of *c-Myc*. In contrast, the second was T(12;15) negative, but had an elevated *N-Myc* expression caused by a paracentric inversion of chromosome 12. Thus, novel mechanisms juxtapose *Ig* and *Myc*-family genes in AID-deficient plasma cell tumors.

CORRESPONDENCE
Michael Potter:
potter@helix.nih.gov

Abbreviations used: aCGH, array comparative genomic hybridization; AID, activation-induced cytidine deaminase; BAC, bacterial artificial chromosome; CNS, central nervous system; DSB, double-strand break; FISH, fluorescence in situ hybridization; qPCR, quantitative PCR; SKY, spectral karyotyping.

Pristane-induced plasma cell tumors and those that develop spontaneously in BALB/c IL-6 transgenic mice carry either T(12;15) translocations between *IgH* and *c-Myc* (1–3) or T(6;15), T(15;16) between *Ig* light chain and *Pvt*-1 (4). These translocations activate and deregulate the transcription of the protooncogene *c-Myc* (5), and they are found in >95% of the plasma cell tumors, strongly suggesting that deregulation of *c-Myc* is a critical, and possibly the initiating, event in their development. Most of the *IgH* breaks occur in the Sμ or Sα regions, although other rare rearrangements or insertions have been previously described (6–10).

Activation-induced cytidine deaminase (AID), which is encoded by the gene *Aicda*, has been shown to be essential for physiological class switch recombination and somatic hypermutation (11–13). Both class switch recombination and somatic hypermutation are associated with the generation of DNA double-strand breaks (DSBs). Two basic models have evolved to explain how AID contributes to the generation of these breaks. The first invokes deamination of cytidine in single-stranded DNA, followed by recruitment of uracil DNA glycosylase or

The online version of this article contains supplemental material.

mismatch repair proteins, leading to the generation of DSB and error-prone repair (14–16). There are also several lines of evidence that favor a second "RNA-editing" hypothesis, which postulates that AID functions as an mRNA deaminase that edits a putative precursor RNA, converting it to an mRNA encoding an endonuclease that cleaves *IgH* switch regions (17, 18).

Consistent with its role in creating DNA breaks in *IgH* switch regions, AID has been implicated in the etiology of canonical *IgH/c-Myc* translocations (19, 20). However, the role of AID in plasma cell tumor development has not been determined. In this study, we ask whether plasma cell tumors can be induced in *Aicda*$^{-/-}$ mice by the intraperitoneal injection of pristane.

Most previous studies of *Aicda*$^{-/-}$ mice used animals raised under specific pathogen–free (SPF) conditions. It was shown earlier that the incidence of pristane-induced plasma cell tumors is strikingly reduced in SPF-raised mice, and that high yields of these tumors require a conventional environment (21). Preliminary experiments with conventionally raised pBALB/c-*Aicda*$^{-/-}$ resulted in deaths of the mice from a wasting syndrome that is attributed to an abnormal composition of gut flora, excessive lymphoid neogenesis (22), and reactivation of latent viruses.

To minimize these complications, we used an accelerated model of tumor induction. Previous studies showed that the time course for pristane-induced plasma cell tumor development was markedly increased in mice carrying a Bcl-2 transgene (23). Furthermore, Cheung et al. showed that the 3′Eκ-Bcl-xL transgene cooperates with enforced expression of *c-Myc* to accelerate plasma cell tumor formation (24). In this study, we confirmed that constitutive expression of Bcl-xL greatly accelerated pristane-induced plasmacytoma development using BALB/c mice carrying a SV40-Eμ-Bcl-xL transgene.

We backcrossed the Bcl-xL transgene onto a BALB/c-*Aicda*$^{-/-}$ background to determine if AID-deficient mice can be induced to develop plasma cell tumors. We report that absence of AID had an inhibitory effect on plasma cell tumor induction by pristane. It resulted in a substantial delay in the emergence of atypical plasma cell tumors that did not grow in ascite form, had altered transplantability, and carried non-canonical translocations between *c-Myc* and *IgH*.

RESULTS

Acceleration and augmentation of plasma cell tumor development in pristane-treated BALB/c-Bcl-xL (Bx) transgenic mice

Mice carrying the SV40-Eμ-Bcl-xL transgene, like Bcl-2 transgenics (25), spontaneously developed a low incidence of plasma cell tumors (19%) with long latencies of >300 d (Fig. 1 A and Table I). Injection of pristane into BALB/c-Bcl-xL transgenic mice resulted in a marked acceleration and greatly increased incidence of plasma cell tumors arising in the oil granuloma (Fig. 1 A). These mice first developed ascites containing tumor cells between 30 and 40 d after injection, and by day 140 77% of the mice had developed plasma cell tumors that were readily transplantable (5/5 tumors grew within 30 d).

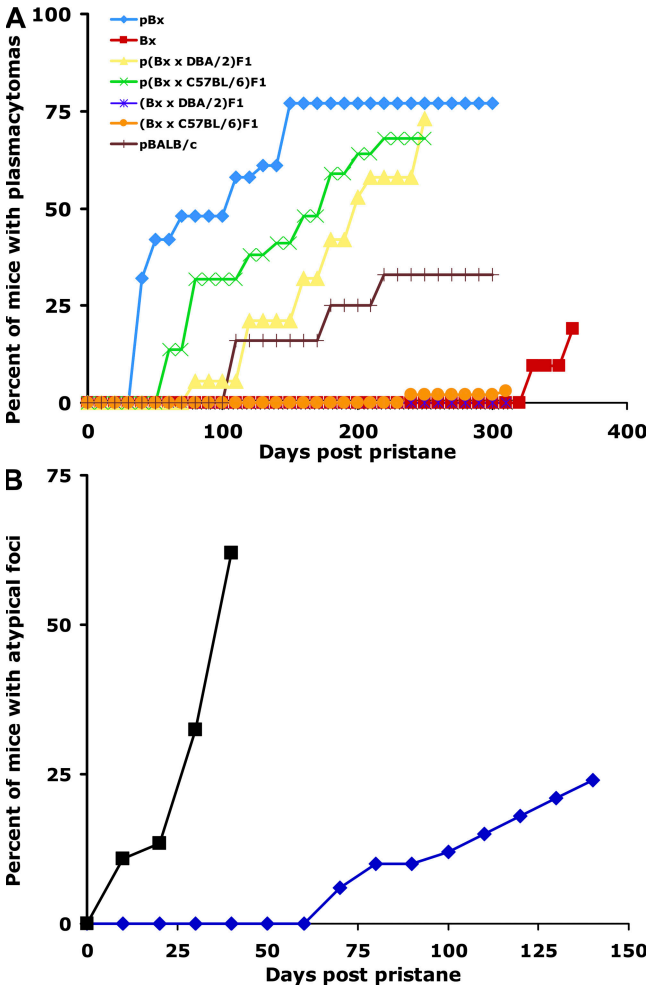

Figure 1. Augmentation and acceleration of pristane (p)-induced plasma cell tumor formation by the Bcl-xL transgene. (A) The Bcl-xL transgene was backcrossed onto BALB/cAnPt. At N5 BALB/c-Bcl-xL (Bx) were crossed to C57BL/6 and DBA/2, and the F1 hybrids were injected with pristane: pBx (diamonds, blue); p(Bx x DBA/2)F1 (triangles, yellow); p(Bx xC57BL/6)F1 (X, green); pBALB/c (+, brown). Nonpristane injected controls: Bx (filled squares, red); (Bx x DBA/2)F1 (squares with an x, lavender); (Bx x C57BL/6)F1 (filled circles, orange). See Table I for numbers of mice and percentages of plasma cell tumors. (B) Incidence of plasma cell tumors as determined by histological appearance of foci, each containing 50 or more atypical plasma cells. Mice with one or more atypical foci were regarded as positive. Squares, black: plasma cell tumors in 23/37 pBx transgenic mice. Diamonds, blue: plasma cell tumors in 8/33 pBx*Aicda*$^{-/-}$ mice.

The BALB/c-Bcl-xL mice were also crossed to C57BL/6 and DBA/2. These strains, as well as their F1 hybrids with BALB/c, are resistant to plasma cell tumor induction by pristane (26) (Fig. 1 A). In contrast, the incidence of plasma cell tumors in mice haploid for the Bcl-xL transgene was greatly increased, even though the latency was prolonged relative to that of pBxBALB/c mice. Thus, the Bcl-xL transgene was

Table I. Summary of induction studies

Figure	Pristane	Background genotype	Bcl-xL transgene	*Aicda* geno-type	PCT/total	Mean latent period	Method of diagnosis
					%	*d*	
1 A	–	BALB/c	+	+	4/21 (19%)	382	Cytofuge
1 A	+	BALB/c N5	+	+	24/31 (77%)	66	Cytofuge
1 A	+	BALB/c N5, LM	–	+	14/33 (38%)	193	Cytofuge
1 A	+	(BALB/c N5 x C57BL)F1	+	+	32/44 (72%)	139	Cytofuge
1 A	+	(BALB/c N5 x C57BL)F1	–	+	3/28 (10%)	269	Cytofuge
1 A	+	(BALB/c N5 x DBA/2)F1	+	+	15/19 (79%)	187	Cytofuge
1 A	+	(BALB/c N5 x DBA/2)F1	–	+	0/19 (0%)	–	Cytofuge
1 B	+	BALB/c	+	+	23/27 (62%)	36	Histology
1 B	+	BALB/c	–	–/–	1/45 (2%)	132	Histology
1 B	+	BALB/c N7	+	–/–	8/33 (24%)	108	Histology

B/c, BALB/c; LM, littermates; N, backcross generation; PCT, plasma cell tumor.

able to augment and accelerate plasma cell tumor development in these genetically resistant strains.

Effects of pristane injection on survival of conventional BALB/c *Aicda*$^{-/-}$ (p*Aicda*$^{-/-}$) mice

Groups of conventionalized *Aicda* $^{-/-}$ mice were raised on a diet with or without metronidazole to control the growth of anaerobic bacteria in the gastrointestinal tract (22) (Table S1 and Fig. S1, available at http://www.jem.org/cgi/content/full/jem.20070882/DC1). At various intervals after the intraperitoneal injection of pristane, p*Aicda*$^{-/-}$ mice began losing weight, developing a hunched posture and ruffled fur. When weight loss or other signs became apparent, the mice were killed and autopsied. Others showed signs of a central nervous system (CNS) disorder, such as hind limb paralysis or ataxia. The cause of the CNS signs was not determined, but could be caused by activation of latent mouse hepatitis virus, which these mice are known to carry (unpublished data). The mean survival time for p*Aicda*$^{-/-}$ mice was 130 d without and 155 d with metronidazole. The incidence of plasma cell tumors in the group without antibiotic was 38% (mean latency of 239 d) and with antibiotic was 32% (mean latency of 177 d). A single developing plasma cell tumor was found in the p*Aicda*$^{-/-}$ mice. Thus, the plasma cell tumors began appearing in AID-competent mice long after most of the corresponding *Aicda*$^{-/-}$ mice had already died. Further, the incidence of plasma cell tumors was very low in the *Aicda*$^{-/-}$ mice that did survive into the period when tumors commonly occur in WT mice.

Induction of atypical plasma cell tumors in pristane-treated BALB/c-Bcl-xL transgenic *Aicda*$^{-/-}$ (pBx*Aicda*$^{-/-}$) mice

To accelerate plasma cell tumor formation, we injected pristane into BALB/c-Bcl-xL transgenic *Aicda*$^{-/-}$ (pBx*Aicda*$^{-/-}$) mice. These mice developed the aforementioned wasting syndrome, and many developed dyspnea caused by greatly enlarged superior mediastinal lymph nodes. These mice also exhibited lymphoid neogenesis (see below). As a result of these threatening complications, most of the mice had to be killed. Notably, none of the mice had ascites. Oil granulomas were found in pBx*Aicda*$^{-/-}$ mice, but in smaller amounts than in pBx*Aicda*$^{+}$ mice, and they did not appear to contain suspicious tumorlike areas. Nonetheless, the oil granuloma tissues were harvested and transplanted into pristane-conditioned BALB/c mice or fixed for histological studies. Unexpectedly, histologic studies revealed that some of these mice had plasma cell tumors in the mesenteric oil granulomas. 8/33 (24.2%) of p*Aicda*$^{-/-}$ mice were found to have evidence of plasma cell tumor formation in oil granuloma tissue after 72–149 d (mean latency of 108 d; Fig. 1 B and Table II). An additional pBx*Aicda*$^{-/-}$ plasma cell tumor, 4987, was discovered in a separate study, but was not included in the incidence figures for this experiment.

Plasma cell tumors induced by pristane characteristically spread from one site to another within oil granulomas. 3 of the neoplasms found in pBx*Aicda*$^{-/-}$ mice involved >15 sites (advanced plasma cell tumors), 4 had 10 or more foci of atypical plasma cells (intermediate), and 2 had only 3–6 foci. The foci were located near or on peritoneal surfaces and involved multiple mesenteric polyplike structures, suggesting possible transperitoneal seeding (27).

The pBx*Aicda*$^{-/-}$ plasma cell tumors exhibited a spectrum of morphological types from lymphocytoid plasma cells (5000) to well-differentiated plasma cells (4451) resembling Russell body cells (Fig. 2). There was also one example of a plasma cell tumor (4885) with morphological features typical of plasma cell tumors of *Aicda*$^{+}$ or WT mice. Finally, consistent with deficiency of switched Ig classes in sera of humans and mice deficient in AID (13), all of these plasma cell tumors were shown by immunohistochemistry to express IgM and Igκ, but no IgA or IgG as is typical of plasma cell tumors from AID-competent mice (unpublished data).

pBx*Aicda*$^{+}$ mice developed plasma cell tumors that were diagnosed by the appearance of tumor cells in the ascites between 50 and 130 d after pristane injection (mean latency of 86 d).

Table II. Characteristics of plasma cell tumors in pBx*Aicda*$^{-/-}$ mice

Mouse#	Post pristane	Oil granuloma no. foci	Transplant to pristane-primed recipient	FISH
	d			
3935	77	20	no growth	+ T(12;15)
4885	72	20	+ 4 mo	+ T(12;15)
4451	102	6	no growth	+ T(12;15)
4961	111	15	+ 4 mo	Inv (12)
4592	149	13	no growth	negative
5000	84	3	no growth	+ T(12;15)
5008	133	13	no growth	+ T(6;15)
5047	135	6	no growth	+ T(12;15)
4987	127	11	no growth	+ T(12;15)

Because none of the pBx*Aicda*$^{-/-}$ mice developed ascites, the diagnosis of plasma cell tumors in these mice had to be made retrospectively by microscopic analyses of tissue sections. To make direct comparisons with other groups, we examined tissue sections from 37 pBx*Aicda*$^{+}$ mice for atypical plasma cell focus development between days 14 and 49 after pristane (Fig. 1 B). Mice with one or more foci were considered positive. The plasma cells in these foci were hyperchromatic and resembled cells characteristic of plasma cell tumors. The mean latency after pristane for tumor development in the 21 positive mice was 36 d.

pBx*Aicda*$^{-/-}$ plasma cell tumors proved to be difficult to transplant, whereas plasma cell tumors of pBx mice were readily transplantable and grew out within 30 d. We consider completely transformed plasma cells to be transplantable. There are several possible explanations for this. First, we were not able to establish the clonality of the primary tumors in pBxAicda$^{-/-}$ mice by immunohistochemistry, PCR, or Southern blotting. Second, in mice with few foci (4451, 5000, and 5047), it is possible that the transplanted tissue fragments did not contain a tumor focus (Table II). Third, the more advanced cases (4885 and 4961) that did grow in transplant differed from pBx*Aicda*$^{+}$ tumors by taking 4 mo to grow out in pristane-conditioned BALB/cAn mice. Furthermore, one of the two more advanced tumors (4961) did not grow out in efforts to passage it a second time. This could be evidence of incomplete transformation.

Both transplantable tumors (4885 and 4961) were established in tissue culture as cell lines. They exhibited a mature plasma cell phenotype (CD45^{-}, CD138^{+}, PC-1^{+}, CD19^{-}, and CD23^{-}), secreted IgM, and were clearly of donor origin, as they were shown to carry the Bcl-xL transgene by PCR analysis and carried both *Aicda*$^{-/-}$ alleles. In contrast to all previously studied mouse plasma cell tumors, both cell lines were found to express CD5 cell surface marker, and 4961 had intermediate expression of CD11b by FACS analysis (unpublished data). We conclude that atypical plasma cell tumors develop in pBx*Aicda*$^{-/-}$ mice and that they appear at a much slower rate than in AID-sufficient mice. pBx*Aicda*$^{-/-}$ plasma cell tumors also differed from tumors of AID-competent mice in their ability to grow in secondary recipients.

Exaggerated lymphoid neogenesis in tissues of pBx*Aicda*$^{-/-}$ mice

When compared with the p*Aicda*$^{-/-}$ mice, the pBx*Aicda*$^{-/-}$ mice had additional complications that were caused by excessive lymphoid hyperplasia in the form of lymphoid aggregates, which were previously described as lymphoid neogenesis (28, 29). Numerous lymphoid aggregates were found in the wall of the small intestine and the lamina propria of the intestinal villi, with some presenting as isolated lymphoid follicles (22, 30).

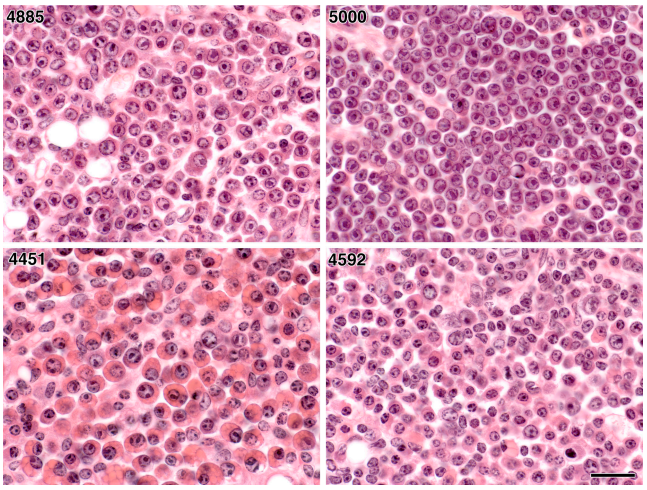

Figure 2. Photomicrographs of four plasma cell tumors arising in pBx*Aicda*$^{-/-}$ mice that show variations in plasma cell morphology. 4885 resembles tumors found in WT mice. The most undifferentiated, 5000, resembles lymphocytoid plasma cells. They have the least amount of cytoplasm, which consists of a thin rim around the nucleus. 4451 contains many cells with Russell body–like features, as well as cells with mature plasma cell morphology. 4961 is an early plasma cell tumor showing many small plasma cells that differ in size from the common types of plasma cell tumors that are well known to contain near tetraploid numbers of chromosomes. Bar, 20 μm.

Many of these aggregates contained germinal center–like structures with a central PNA$^+$ zone surrounded by B220$^+$ lymphocytes. These aggregates were rarely seen in p*Aicda*$^{+/-}$ mice. Most of the p*Aicda*$^{-/-}$ mice had splenomegaly, along with enlarged mesenteric lymph nodes and Peyer's patches. Many developed dyspnea caused by greatly enlarged superior mediastinal lymph nodes resulting from the transport of pristane oil out of peritoneal space or, in some cases, to the formation of lymphoid tissues in the lungs (Fig. S2 A, available at http://www.jem.org/cgi/content/full/jem.20070882/DC1).

An important characteristic of the oil granulomas in pBx-*Aicda*$^{-/-}$ mice was the presence of variable, but usually large, numbers of these lymphoid aggregates. Most contained PNA$^+$ lymphocytes and resembled the aggregates of lymphoid neogenesis (Fig. S2, B–D). Many of the neogenic lymphoid aggregates were associated with plasma cell formation in the oil granuloma, suggesting that these might also represent initiating sites for plasma cell tumor development. However, a clear histological link to plasma cell tumor formation was not found.

Most plasma cell tumors of pBx*Aicda*$^{-/-}$ mice carry translocations between *IgH* and *c-Myc*

Focal plasma cell tumors were first found in histological sections stained with hematoxylin and eosin. The corresponding sites in serial sections were examined by fluorescence in situ hybridization (FISH), and photographed, and the number of signals per cell was recorded. Intact diploid nuclei exhibited 2 red (*IgH*) and 2 green (*c-Myc*) signals, and cells with T(12;15) had 1 red, 1–2 green, and 1 fused (yellow) signal (Fig. 3, A and B). Many nuclei had fewer signals, as all chromosomes were not uniformly included in the plane of the 5-μm section. Cells were examined using 3D view (Fig. 3, C and D), and *IgH/c-Myc* gene colocalization was confirmed.

The proportion of cells with fusion signals in pBx*Aicda*$^{-/-}$ plasma cell tumors (3935, 4451, 4987, 4885, 5000, and 5047) ranged from 34 to 63%. In pBx*Aicda*$^{+/-}$ plasma cell tumors, the proportions ranged from 29 to 57% (Table S2, available at http://www.jem.org/cgi/content/full/jem.20070882/DC1). Samples from different parts of a tumor showed variations in the proportion of positive cells, which may be caused by varying contributions of stromal or other nontumor cells.

As controls, five samples of lymphoid hyperplasia or extramedullary myelopoiesis, taken from the same oil granuloma tissue sections, showed 0–2.6% of cells with a fusion signal. These data were used to establish a value of 4.1% (four standard deviations above the mean) as identifying translocation-bearing plasma cell tumors. Based on these calculations, three additional plasma cell tumors from pBx*Aicda*$^{-/-}$ mice (4961, 5008, and 4592) were scored as T(12;15) negative.

Tissue sections of tumors negative for T(12;15) were hybridized with probes specific for *IgK* on chromosome 6 and for *c-Myc* to detect T(6;15), which is a translocation found at lower frequency than T(12;15) in plasma cell tumors of AID-sufficient mice. Tumor 5008 was positive for *Igκ/c-Myc* colocalization, with 55% of cells positive for fusion signals, this is in comparison to a plasmacytic focus from the same section, with only 3.5% positive cells.

PCR and Southern blot hybridization studies of primary plasma cell tumors and cell lines

The frequency of T(12;15) in pristane-induce plasma cell tumors of WT mice is ∼80% (31).The vast majority of either

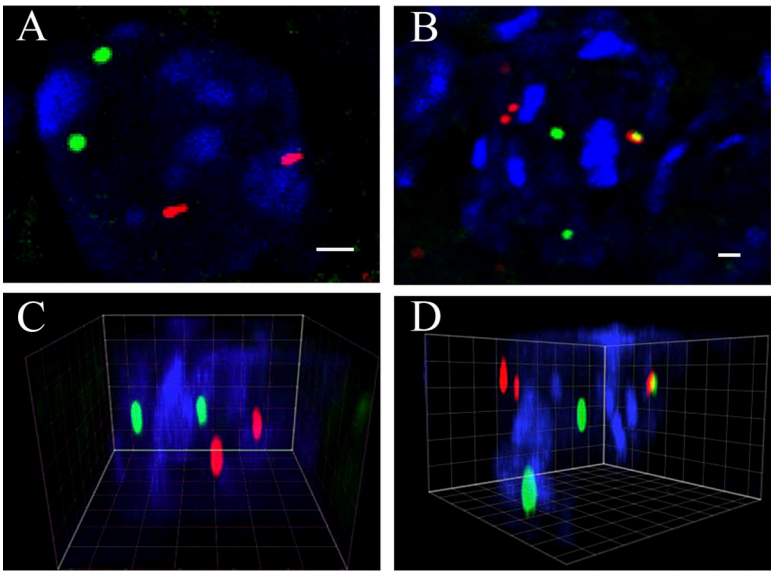

Figure 3. Interphase FISH on tissue sections showing *IgH/c-Myc* colocalization in pBx*Aicda*$^{-/-}$ plasma cell tumor 4885. (A and C) Two- and three-dimensional photomicrographs of interphase nuclei from a cell with no evidence of T(12;15) translocation: two red (*IgH*) and two green (*c-Myc*) signals. (B and D) A cell with a fused signal indicative of T(12;15), doublet Red (*IgH*) resulting from hybridization to two sister chromatids, and two green (*c-Myc*) signals. Grid, 1 μm. Bars, 1 μm.

der(12)T(12;15) or der(15)T(12;15) breakpoints can be amplified by PCR (32, 33). To determine the nature of the translocations in pBx*Aicda*$^{-/-}$ plasma cell tumors, we performed PCR reactions using long PCR (covering VDJ-Eμ, Cμ, Cγ1, Cγ2b, Cγ2a, Cε, and Cα), as well as PCR with switch region degenerate primers. We were unable to amplify products containing *c-Myc* and *IgH* chimeric sequences (unpublished data). As controls, we analyzed seven pBx*Aicda*$^{+/-}$ tumors, five of which were positive (Table S3, available at http://www.jem.org/cgi/content/full/jem.20070882/DC1). Thus, the

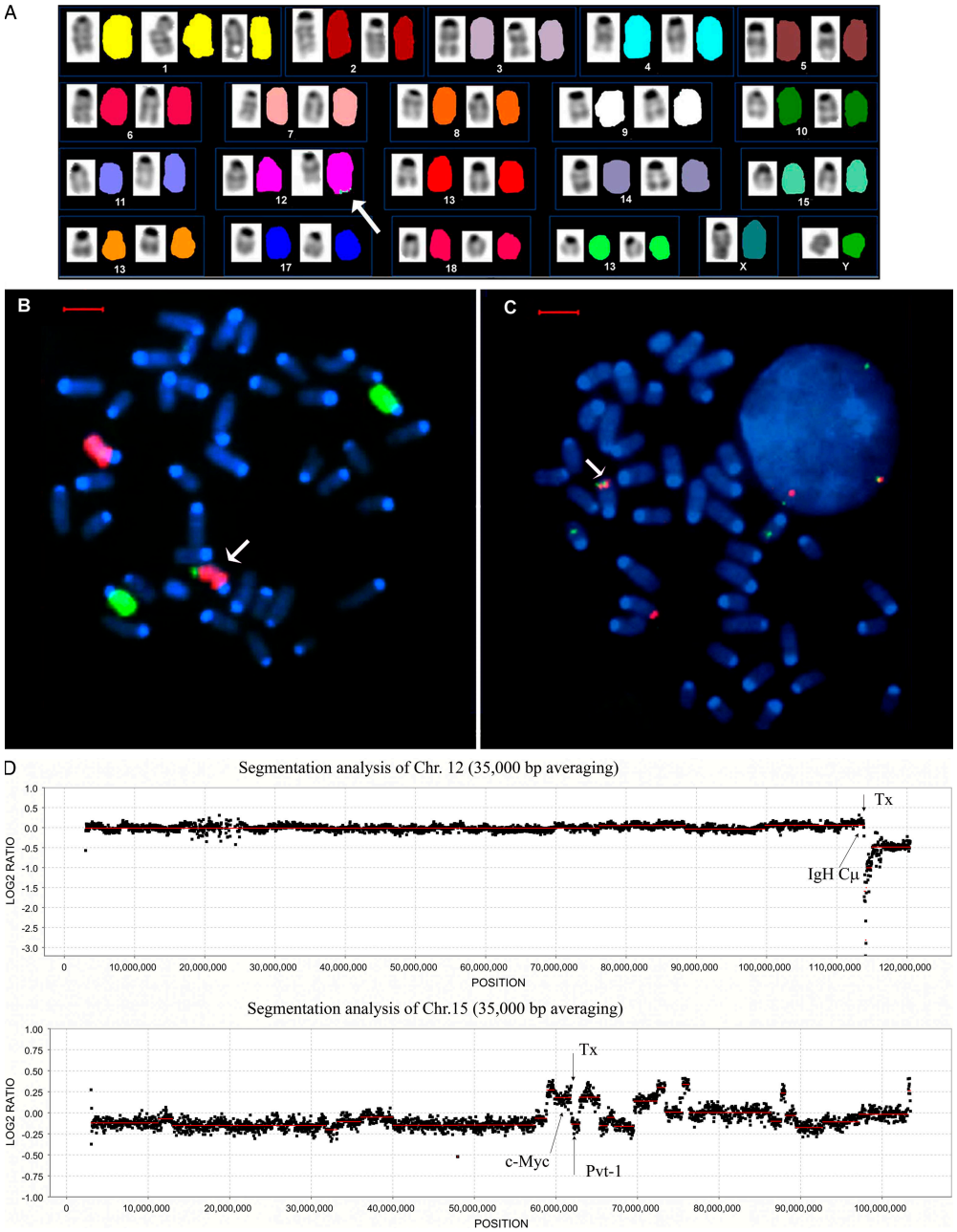

Figure 4. Molecular and cytogenetic analysis identifies the T(12;15) chromosomal translocation in the pBx*Aicda*$^{-/-}$ cell line, 4885. (A) A representative karyotype of cell line 4885 analyzed by SKY shows a subtle translocation involving chromosome 12 and 15 as indicated by the arrow. (B) FISH using whole chromosome painting probes confirms a T(12;15) (arrow). Metaphase chromosomes are DAPI-stained. The normal chromosome 12 is depicted in red, and the normal chromosome 15 is shown in green. (C) FISH with gene-specific probes confirmed the involvement of *c-Myc* and *IgH* in the chromosomal rearrangement. Within the DAPI-stained metaphase, probes for *c-Myc* (green) and *IgH* (red) are colocalized on the abnormal chromosome (arrow). Additionally, *c-Myc* signals are present on the normal chromosome 15, whereas the signal for the *IgH* gene appears on the normal chromosome 12. (D) aCGH profile of the 4885 cell line. Locations of *IgH Cm* (chromosome 12, top plot) and *Pvt-1* (chromosome 15, bottom plot) are indicated by arrows pointing up. Translocation breakpoints (Tx) are depicted by arrows pointing down. Bars, 5 μm.

translocations in pBx*Aicda*$^{-/-}$ mice take place in unusual locations and are unlikely to involve switch regions.

Southern blots performed with DNA isolated from cell lines 4885 and 4961 showed that the *c-Myc* gene was in germline configuration and not amplified (unpublished data). Analysis of J_H rearrangements in these tumors revealed the absence of a germline band and the presence of two rearranged bands in the translocation-negative cell line (4961) and a single rearranged band in the T(12;15)-positive cell line (4885; Fig. S3, available at http://www.jem.org/cgi/content/full/jem.20070882/DC1). This indicates that in 4885, one copy of the J-C intron was completely lost as the result of a nonreciprocal T(12;15) translocation.

Consistent with the Southern blot data, 4885 carried and expressed a single rearranged heavy chain allele (Vh J558, 17-DSP2.13-Jh4). 4961 carried both alleles; one productively rearranged (J558.41-DSP2.7-Jh2) and another with stop codons (J558.41-DSP2.2-Jh2). DNA sequences of expressed $V_HD_HJ_H$ and V_kJ_K genes had no mutations (unpublished data).

pBx*Aicda*$^{-/-}$ plasma cell tumor cell lines exhibit atypical *IgH/Myc* rearrangements

The pBx*Aicda*$^{-/-}$ cell line derived from tumor 4885 was analyzed by spectral karyotyping (SKY) and showed a near diploid karyotype of 39−42, XY, +1, +15, der(12)T(12;15) in at least 15 metaphase spreads (Fig. 4 A). The translocation was rather subtle because the telomeric portion of chromosome 15 appeared smaller then usual. FISH analysis using whole chromosome painting probes for mouse chromosome 12 and 15 confirmed the presence of a T(12;15) (Fig. 4 B). Further analyses with gene-specific probes identified a juxtaposition of *IgH* and *c-Myc* (Fig. 4 C), the absence of a reciprocal chromosome der(15)T(12;15) and the presence of an extra copy of "normal" chromosome 15. Therefore, a nonreciprocal T(12;15) may have originated in a cell with a trisomy of chromosome 15, which is a frequent occurrence in mouse B cell and T cell lymphomas, but is almost never seen in diploid mouse plasma cell tumors (34).

Because of the unbalanced T(12;15) in 4885, we used NimbleGen's high-resolution array comparative genomic hybridization (aCGH) to map translocation breakpoints. Analysis of an array CGH profile of chromosome 12 shows gross deletions in the 5′*IgH* locus, which is typical for VDJ recombination events (Fig. 4 D, top plot). Additionally, it shows the loss of one copy of the telomeric portion of chromosome 12 ($\log_2$ ratio of −0.5) starting at ∼650 bp upstream of the first exon of *IgH Cμ*, which indicates the approximate position of the translocation breakpoint (Fig. 4 D and Fig. S4, available at http://www.jem.org/cgi/content/full/jem.20070882/DC1). This deletion is also consistent with the loss of der(15)T(12;15).

In contrast, alterations of chromosome 15 appear to be much more complex and show six regions of gains, including one in the telomeric portion (Log_2 ratio of 0.25; Fig. 4 D, bottom plot). This finding suggests multiple deletions of der(12). We used FISH with bacterial artificial chromosomes (BACs) aligned to the regions of gains and reconfirmed their presence on all copies of chromosome 15 and der(12)T(12;15). BAC 62I2 that corresponds to the distal portion of chromosome 15 in the region showing no gain, hybridized only to 2 "normal" copies of chromosome 15. The schematic structure of der(12) chromosome is presented in Fig. S4.

Because the location of the translocation breakpoint was scrambled for chromosome 15 and straightforward for chromosome 12, we resorted to inverse PCR using *IgH Cμ* primers to amplify the junction. Sequence analysis identified the breakpoint location on chromosome 12 just 211 bp upstream of the first exon of *IgH Cμ*, which is very close to the breakpoint predicted by aCGH (see above). The chromosome 15 breakpoint was ∼75 kbp downstream of *c-Myc*, which was joined with *IgH* in a head-to-tail orientation that is unusual for T(12;15) translocations. This finding suggests that chromosome 15 underwent a paracentric inversion involving the *c-Myc* locus before or during illegitimate recombination with chromosome 12 (Fig. S4). Consistent with the aCGH data, the *Pvt-1* locus was allocated to der(15) and cannot be detected with RP23-96F18 BAC on der(12) (Fig. S4). ABPC60 is the only known plasma cell tumor with a T(12;15) to have the breakpoint 3′ of *c-Myc* (9). Moreover, before this study, the closest known breakpoint to *IgH Cμ* (914 bp 5′) was in a BALB/c pristane-induced tumor PCT 4130 (unpublished data). We conclude that the breakpoint location in 4885 is atypical compared with other mouse plasma cell tumors with T(12;15).

For the pBx*Aicda*$^{-/-}$ cell line 4961, 10 complete metaphases were analyzed by SKY and showed a near diploid karyotype of 40, X, T(1;10), +6, In(12), T(10;1) (Fig. 5 A). One copy of chromosome 12 showed an abnormal inverted DAPI pattern suggestive of a paracentric inversion (Fig. 5 B). We performed additional metaphase FISH studies to identify the genes affected by the inversion. Using FISH with 3′*IgH*- (green) and 5′*IgH*-specific (red) probes, we uncovered the relocation of *IgH* 3′ locus control region from it's usual telomeric site toward the centromere (Fig. 5 C) and colocalization of the 3′*IgH* probe (green) with a BAC probe for *N-Myc* (red) on inv(12) (Fig. 6 D). Ideograms of the normal and the inverted chromosome 12 are drawn in Fig. 5 D. An aCGH analysis of chromosome 12 did not reveal any sizable deletions associated with the inversion or amplifications (unpublished data). Consistent with the PCR and Southern blot analysis data described previously, we propose that the inversion must have occurred upstream of the rearranged VDJ segment. It is not yet clear if the inversion involved the expressed or the nonexpressed allele. The break site in the vicinity of *N-Myc* must have occurred within 200 kbp telomeric to the gene. A proposed structure of this novel chromosome 12 inversion in 4961 is presented in Fig. S4.

Up-regulated expression of *c-Myc* or *N-Myc* in pBx*Aicda*$^{-/-}$ cell lines

To establish that the observed genomic rearrangements, indeed, resulted in activation of adjacent oncogenes, we compared

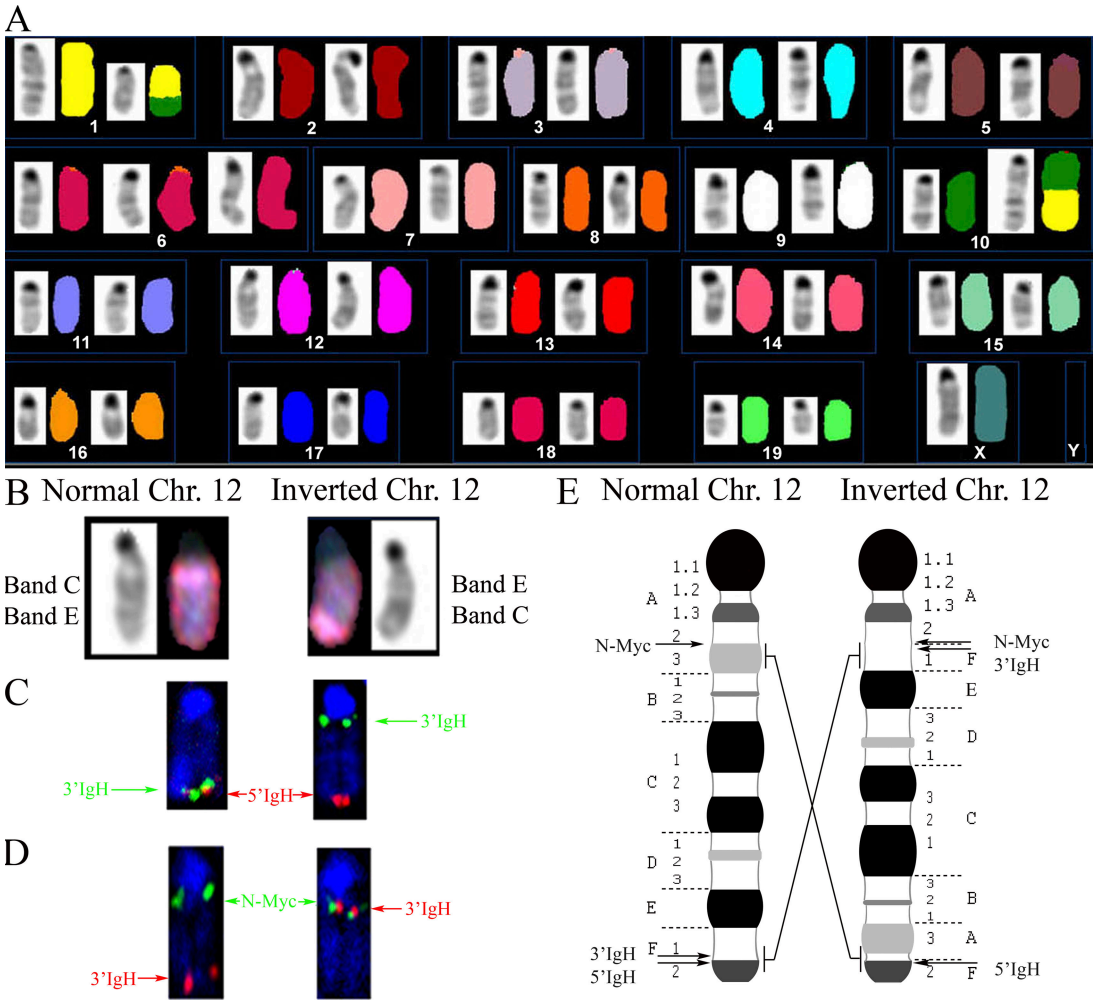

Figure 5. Cytogenetic analysis of pBx*Aicda*$^{-/-}$ cell line 4961. (A) SKY identifies a reciprocal T(1;10) translocation and trisomy 6. (B) Inverted DAPI staining and spectral image of normal (left) and inverted (right) chromosome 12 showing different band pattern on the inverted chromosome. (C) FISH with 3′*IgH* (green) and 5′*IgH* (red) gene-specific probes identifies one normal chromosome 12 (left) and breakage of the *IgH* locus on the other chromosome 12 (right) as the result of a paracentric inversion. (D) FISH shows colocalization of 3′*IgH* (green) and *N-Myc* (red) signals on inverted chromosome 12 (right) and their usual location at opposing ends on normal chromosome 12 (left). (E) Ideograms showing a normal chromosome 12 (left) and chromosome 12 with a paracentric inversion (right).

expression of *c-Myc* and *N-Myc* mRNA in pBx*Aicda*$^{-/-}$ and pBx*Aicda*$^{+/+}$ cell lines using quantitative PCR (qPCR). Expression of *c-Myc* was comparably elevated in all cell lines except for 4961 that expressed a high level of *N-Myc* message (Fig. 6).

DISCUSSION

In this study, we showed that plasma cell tumors can be induced in pristane-treated BALB/c-Bcl-xL *Aicda*$^{-/-}$ mice. These tumors, however, are characterized by a reduced frequency and prolonged latency when compared with plasma cells tumors of pristane-treated AID-competent mice. The plasma cell tumors in the pBx*Aicda*$^{-/-}$ mice also differed from those arising in pBx*Aicda*$^{+}$, as six were apparently in early or intermediate stages of progression and most could be diagnosed only retrospectively by studies of histologic sections. The pBx-*Aicda*$^{-/-}$ mice did not develop ascites, a process that facilitates diagnosing plasma cell tumors by paracentesis. Thus, one of the important signs of tumor development was not present. Finally, most of these tumors had not progressed to become fully autonomous malignancies. In summary, AID is essential for the usual development and progression of pristane-induced plasmacytomas. Nevertheless, atypical plasma cell tumors can arise in the absence of AID.

Using interphase FISH in paraffin sections, we found evidence of T(12;15) chromosomal translocations in 6 of the 9 pBx*Aicda*$^{-/-}$ tumors studied (Table II). In these samples, 35–63% of the cells in the tumor-containing regions exhibited fusion signals that were interpreted as indicative of T(12;15) translocations. Our initial expectation was that in the absence of AID the *Igκ/Pvt-1* recombination would be preferred. However, we found a T(6;15) in only one tumor, 5008.

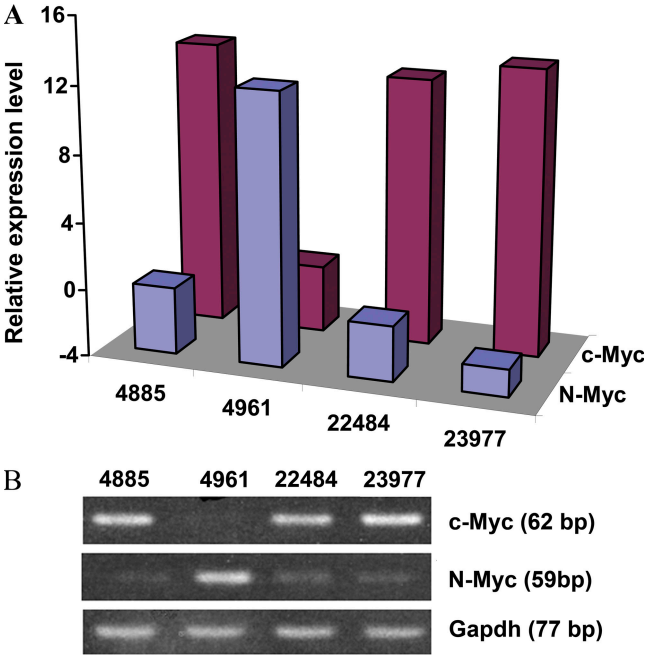

Figure 6. Comparison of *c-Myc* and *N-Myc* transcript levels in pBx*Aicda*$^{-/-}$ cell lines 4961 and 4885 to pBx*Aicda*$^{+/+}$ controls. (A) Summary of qPCR analysis of *c-Myc* and *N-Myc*. Numbers indicate the log2 transformed fold change. Data are mean expression from three independent experiments. (B) Agarose gel electrophoresis of qPCR products. 10 μl of qPCR reaction were loaded on 2% agarose gel and visualized by ethidium bromide staining.

A surprising finding was the activation of *N-Myc* by a paracentric inversion of chromosome 12 in tumor 4885. The sole previous example of *N-Myc* activation and deregulation in mouse plasma cell tumors resulted from the juxtaposition of *Igκ* and *N-Myc* loci in an exceptional mouse plasma cell tumor, ABPC-132, which carries a reciprocal T(6;12) translocation (35). Functional homology between *N-Myc* and *c-Myc* in mouse plasma cell tumor development was previously shown (36). However, *N-Myc* is normally expressed only during the early stages of B cell development, and was found to be coamplified with *IgH* in B cell progenitor tumors that develop in mice deficient for both *p53* and *Artemis* (37). Thus, the majority of *Aicda*$^{-/-}$ plasma cell tumors similar to those developing in their AID-sufficient counterparts are predisposed to T(12;15) translocations.

Unniraman et al., using highly sensitive PCR methodologies, recently studied lymphoid tissues in pristane-treated BALB/c *Aicda*$^{-/-}$ mice to determine if they contained evidence of switch-related T(12;15) (38). Sequences of the junctional fragments obtained from the tissues harvested at 2–4 wk after pristane showed that breakpoints occurred in *IgH* switch regions. They did not find similar PCR fragments 3–5 mo later. It was not determined if these tissues contained plasma cell tumor cells. The explanation for these findings awaits further clarification. Although we did not study the early response to pristane, we were not able to detect *IgH/c-Myc* illegitimate recombinations in five samples containing pBx*Aicda*$^{-/-}$ plasma cell tumors by using PCR primers used in the Unniraman study or any other primer combination with the exception of Cδ and Cγ3 (Table S4, available at http://www.jem.org/cgi/content/full/jem.20070882/DC1). Our results are in agreement with those of Ramiro et al. (19), who, using another plasma cell tumor induction system, did not detect canonical *IgH/c-Myc* translocations in IL6-transgenic *Aicda*$^{-/-}$ mice.

Molecular and cytogenetic analyses of illegitimate recombinations in 4885 and 4961 pBx*Aicda*$^{-/-}$ cell lines showed no involvement of switch regions or sequences in close proximity to *c-Myc*. This differs from most T(12;15)-positive plasma cell tumors in AID-competent mice (5). A mechanism for generating "untargeted" single-strand DNA breaks and DSB, one that does not depend on special features of switch regions and also involves *c-Myc*, is a potential explanation for our findings. This possibility is supported by earlier studies showing that occasional pristane-induced plasma cell tumors in BALB/c mice have unusual rearrangements of *c-Myc* and *Ig* genes (6–10). Although our experiments confirm the importance of AID in mediating canonical *IgH/c-Myc* translocations, they also establish the existence of additional mechanisms that can lead to illegitimate recombination of *Ig* genes with an oncogene in the absence of AID.

Several studies have described B cells and B cell lymphomas with "unusual" illegitimate recombinations of chromosomes 12 and 15. These studies have used mice with two types of genetically engineered abnormalities. The first involved mice deficient in proapoptotic signaling as a result of homozygosity for a *p53* knockout or by constitutive expression of an antiapoptotic gene, either *Bcl-2* or *Bcl-xL*. The second category is associated with defects in genes involved in DNA damage control (*scid*, *ATM*, *H2AX*, *53BP-1*, and *Nbs-1*) or in nonhomologous end joining (*XRCC4*, *Ligase IV*, *Ku70/80*, DNA *PKcs*, and *Artemis*) (39–46). Tumors associated with these defects predominantly occurred in pro–B cells and contained *IgH/c-Myc* chromosomal translocations. Amplifications, termed complicons, that generated additional illegitimate *IgH/c-Myc* recombinations, sometimes three-way, have also been described in these tumors (41, 47–49). It was proposed that the DSBs leading to these illegitimate recombinations were associated with RAG1/2 activity, as they occurred between V_H and Cμ (41, 47, 48). The mechanism of DNA end joining in these tumors may involve the recognition of microhomologies (50, 51).

Alternative pathways of generating DSBs may target the genomes of B cells, and could be responsible for the aberrant generation of T(12;15) seen in pBx*Aicda*$^{-/-}$ mice. It has been shown that microenvironments that produce oxidants may cause DSBs or lead to neoplastic transformation (52, 53). The pristane-induced oil granuloma in BALB/c mice contains an abundance of neutrophils, particularly in the early stages of its formation, which generate oxidants and other products that have been shown to damage DNA (54). Shacter et al. cocultured plasma cell tumor cells with purified neutrophils in vitro

and found DNA damage in the target cells (55). Some oxidants may arise from endogenous metabolism (56, 57). Also the "endogenous DSB" process occurs during normal DNA replication generating an estimated 50 DSB/nucleus in a cell cycle (58). We are currently unaware of the tissue site in which these DSBs take place. It could be in an extraperitoneal site, such as bone marrow, spleen, or gut-associated lymphoid tissue, or in the oil granuloma itself.

The roles played by enforced expression of Bcl-xL or Bcl-2 in the B lineage and the mechanisms by which they contribute to accelerating plasma cell tumor development are not established. The Bcl-xL transgene, as shown by Fang et al. (59), acts during early B cell development in the bone marrow to give a 4–5 fold expansion of the pro-B cell compartment and permits the survival of pro-B cells that have undergone nonproductive V-D-J rearrangements and extensive D_H or J_H deletions (59, 60). Transgenic Bcl-xL may also exert important effects in peripheral B cells and plasma cells.

In this study, enforced expression of Bcl-xL under the control of the Eμ enhancer and SV40 promoter activates and expresses an antiapoptotic protein, and it acts as a functional equivalent to homozygosity for a null mutation of *p53*. Although the pathway of action of p53, a transcriptional transactivator, and Bcl-xL, an inhibitor of mitochondrial apoptosis (61), may differ, they potentially accomplish a common end result, which is a failure to eliminate cells that have experienced illegitimate recombinations, which may mark the initiation of neoplastic progression. It should be noted, however, that p53 has many other functions such as governing cell cycle checkpoints and DNA replication (62). In addition, p53 deficiency may promote DNA amplifications (63, 64). Ramiro et al. have postulated that there may be a surveillance mechanism mediated by p53 for detecting and eliminating cells that carry translocations (20). The constitutive expression of the antiapoptotic factor Bcl-xL may promote the survival of cells with T(12;15) that express relatively large amounts of Myc that otherwise would drive the cells into apoptosis (65, 66). B cells that harbor these translocations are able to progress slowly into atypical plasma cell dyscrasias reminiscent of indolent states of B cell neoplasia in humans. We conclude that rapid development of malignant plasma cell tumors with reciprocal T(12;15) does require AID, and that in AID deficiency other, less efficient mechanisms can be used to bring *c-Myc* and *Ig* genes into juxtaposition. The reason why recombinations between *IgH* and *c-Myc* occur so regularly in mouse plasma cell tumor formation is thought provoking and, as yet, an unexplained problem.

MATERIALS AND METHODS

Mice. All animals were maintained under NCI IACUC-approved protocols LG023, LG024, and LG025. The mice were fed Purina Mouse Chow 5001 ad libitum and sterilized acidified drinking water. The SV40-Eμ-Bcl-2 transgene was originally developed by Strasser et al. (25) and modified by Grillot et al. (67) by replacing human Bcl-2 with human Bcl-xL. The SV40-Eμ-Bcl-xL transgene, which was originally developed on hybrid backgrounds, was introgressively backcrossed onto conventionally raised BALB/cAnPt mice for six generations in the Laboratory of Genetics (NCI) to generate BALB/c-Bcl-xL transgenic mice. The *Aicda*$^{-/-}$ mice developed by Muramatsu et al. (12) were backcrossed four or more generations onto BALB/c(Kyoto) in Kyoto University and transferred to the NCI in 2003 as SPF mice. In 2004, they were introduced into the NCI conventional facility, where they were maintained in filter-top cages and fed sterile water and a bacon-flavored diet that contained 138 mg/kg metronidazole (Bioserve) to control the microbial flora. BALB/cAnPt-Bcl-xL transgenic mice were crossed to BALB/c(Kyoto)-*Aicda*$^{+/-}$ mice at backcross N4, and the F1 hybrids were crossed to each other to produce F2. The following six genotypes were obtained: Bcl-xL$^{+/-}$ *Aicda*$^{+/+}$, $^{+/-}$, and $^{-/-}$; WT *Aicda*$^{+/+}$, $^{+/-}$, and $^{-/-}$. Mice of all six genotypes were inoculated intraperitoneally with 0.4 or 0.5 ml pristane (Aldrich Chemicals) at 2 mo of age, and a second injection of pristane was given 60 d later.

Sample preparation. Tissues were fixed in Fekete's modified Telleysniczky's fluid (70% ethanol/formalin/glacial acetic acid in 20:2:1 parts) for 12–48 h and transferred to 70% ethanol in buffered saline. These specimens were embedded in paraffin and sectioned at 4–5 μm by HistoServ. To prepare metaphase chromosomes ~10^7 cultured cells were first lysed and then fixed in 3:1 methanol/acetic acid solution. An aliquot of the suspension was dropped onto a glass slide in a controlled temperature (20–25°C) and humidity (45–55%) environment of a Thermotron. Total RNA and genomic DNA were isolated according to the manufacturer's instructions using TRI reagent (Sigma-Aldrich) and Purigene system (Gentra Systems) correspondingly. cDNA was obtained using a kit from Roche.

Plasma cell tumor diagnosis. Plasma cell tumors in pristane-treated BALB/c mice were diagnosed using Wright-Giemsa–stained cytofuge preparations of ascites. The presence of 10 tumor cells per field was scored as a positive. Most positive mice lived for several weeks, and the number of tumor cells increased to >100 per cytofuge field. Because pBx*Aicda*$^{-/-}$ mice did not develop ascites, we used hemotoxylin and eosin–stained sections of oil granulomas to determine the number of foci with 50 or more atypical plasma cells.

Transplantation and in vitro culture. Tumor transplants were initiated by the injection of finely minced oil granuloma tissue into syngeneic BALB/cAnPt mice that had been injected intraperitoneally with 0.2–0.5 ml pristane 1–15 d before transplantation. Cell lines were established from generation 1 transplants by culturing in complete RPMI 1640 medium supplemented with 10% fetal calf serum and 10 ng/ml of IL-6. To ensure that the cell lines were not derived from plasma cell tumors of host origin, the tumor tissues were shown by PCR to carry the human Bcl-xL transgene (68) and both targeted alleles of *Aicda* (12).

Immunohistochemistry, ELISA, and FACS. PNA (Vector Laboratories), anti-B220 (BD Bioscience), -IgM, -IgG, -IgA, and -Igκ (Southern-Biotech) were all conjugated to biotin and reacted directly with sectioned tissue, followed by avidin conjugated to either alkaline phosphatase or peroxidase. Standard ELISA isotyping techniques were applied using mouse serum or concentrated tissue culture supernatant as the antigen at an initial dilution of 1:500. We used goat anti–mouse IgA, IgG_1, IgG_{2a}, IgG_{2b}, IgG_3, and IgM HRP-conjugated antibodies (SouthernBiotech). Cell surface markers were analyzed using a FACSCalibur (Becton Dickinson) after the cells were stained with FITC-, PE-, APC-, or PerCP-conjugated antibodies specific for mouse CD45, CD19, CD138, PC-1, CD23, CD5, and CD11b (BD Biosciences).

Cytogenetic analysis of plasma cell tumors. SKY was performed as previously described (69). SKY image acquisition was performed using the SpectraCube SD200 (Applied Spectral Imaging) connected to an epifluorescence microscope (DMXRA; Leica). Image analysis was done using SKYVIEW program version 1.6.2 (Applied Spectral Imaging). FISH was performed on metaphase chromosomes and interphase nuclei according to standard protocols (http://www.riedlab.nci.nih.gov/protocols.asp#h3) using whole-chromosome

painting probes, as well as gene-specific probes for *IgH* and *c-Myc*. The mouse whole-chromosome paints were labeled by degenerate oligonucleotide primer PCR. Mouse chromosome 12 was labeled with Biotin (Roche) and detected with streptavidin-Cy3 (GE Healthcare), whereas mouse chromosome 15 was directly labeled with Spectrum Green (Vysis). The images were acquired using a DMRXA epifluorescence microscope equipped with a Sensys charge-coupled device camera (Roper Scientific).

BAC clones containing *c-Myc* located on mouse chromosome 15D2-3 (D15Mit17), *Pvt1* gene adjacent to *c-Myc* (RP23-96F18), the Cγ3-Cα constant regions of 3′*IgH* on chromosome 12F1 (189A22), 5′*IgH* variable region on chromosome 12F2 representing the distal end of the V_H cluster (VJ588; V_H-224M14, provided by M. Takizawa, National Institute of Arthritis, Musculoskeletal and Skin Diseases [NIAMS], Bethesda, MD), *IgK* on chromosome 6C2 (RP23-435I4), *N-Myc* on chromosome 12A2 (RP23-246B9; provided by C. Yan, Harvard Medical School, Boston, MA), and 240 kb telomeric to *N-Myc* (RP23-225P23) were labeled using digoxygenin or biotin-nick translation kits (Roche). Detection was performed using streptavidin Alexa Fluor 568 (Invitrogen) and sheep anti–digoxigenin-fluorescein FAB fragments (Roche). Nuclei were counterstained with DAPI using Vectashield mounting medium (Vector Laboratories).

Confocal z stack images of tissue sections taken at 0.5-μm intervals were acquired on a fluorescent microscope (IX81; Olympus Optical) with a 100× oil lens using Slidebook software v.4.1.0.16 (Intelligent Imaging Innovations). All images were deconvolved, and merged pseudocolor maximum projections were generated. Using the ImageJ program (http://rsb.info.nih.gov/ij), the DAPI-stained nuclei in the photographic field were outlined and numbered. Each nucleus was evaluated for the presence of red (*IgH*), green (*c-Myc*), and yellow (fused) signals. Nuclei were counted in 1–3 photographic fields, and the proportion of nuclei with fusion signals was determined.

aCGH. High-resolution CGH analysis was performed by NimbleGen Systems using part of a whole-mouse genome tiling set, including chromosome 12 (3,027,081–120,462,673) and chromosome 15 (3,000,426–103,492,450). The array design was based on National Center for Biotechnology Information Build 36 of the mouse genome sequence, and median probe spacing was 656 bp. Kidney DNA from a pBx*Aicda*$^{-/-}$ mouse was used as a reference.

PCR and qPCR. PCR on genomic DNA from pBx*Aicda*$^{+/-}$ and pBx*Aicda*$^{-/-}$ plasma cell tumors was performed using previously published procedures (3, 32). EcoRI-digested and self-ligated DNA from tumor cell lines was subjected to inverse PCR, as previously described (70). For complete primer sequences see Table S4. We used degenerate primers to amplify rearranged heavy and light chain variable genes (36). Direct sequencing of PCR products was performed by the NCI sequencing core facility.

For qPCR, 2 ng cDNA was amplified using SYBR Green PCR Master Mix (Applied Biosystems) and 0.33 μM each of forward and reverse primer on a sequence detector system (ABI PRISM 7900HT; Applied Biosystems). Primers for qPCR were designed using the Primer Express software (Applied Biosystems) and synthesized at BioServe Biotechnologies.

The primer sequences were as follows: c-Myc-F1154: 5′-TGAAGCGCAGCTTTTTTGC-3′, c-Myc-R1215: 5′-GGCCTTTTCGTTGTTTTCCA-3′, N-Myc-F1398: 5′-CTGAGCTGGTGAAGAACGAGAA-3′, N-Myc-R1437: 5′-CTCGGTGGCCTTTTTCAAGA-3′, GAPDH-F, 5′-TGTGTCCGTCGTGGATCTGA-3′, GAPDH-R, 5′-CCTGCTTCACCACCTTCTTGAT-3′. All samples were tested in triplicate, and mean values were used for quantification. Analysis was performed using SDS version 2.2 software (Applied Biosystems) according to the manufacturer's instructions. Samples were normalized using the housekeeping gene *Gapdh*. The comparative CT method (ΔΔCT) was used for quantification of gene expression.

Southern blot analysis. Southern blotting was performed using standard procedures. Kidney DNA from a tumor-free pBx*Aicda*$^{-/-}$ was used as a control for DNA obtained from the 4885 and 4961 cell lines. DNAs were digested overnight with EcoRI or HindIII, and hybridization was performed with P^{32}-labeled mo*Myc* #303 or pJ11 probes provided by K. Huppi (NCI, Bethesda, MD). Images were scanned using the Typhoon imaging system (Molecular Dynamics).

Online supplemental material. Fig. S1 is a graphical representation of survival and tumor incidence in pristane-injected pBx*Aicda*$^{-/-}$ mice with or without antibiotic treatment. Fig. S2 presents histological evidence of exaggerated lymphoid neogenesis in lungs and oil granuloma tissue of pBx*Aicda*$^{-/-}$ mice containing multiple germinal center–like structures. Fig. S3 shows clonal Jh rearrangements in pBx*Aicda*$^{-/-}$ cell lines identified by Southern blotting. Fig. S4 is a scheme depicting the molecular structure of genetic alterations in pBx*Aicda*$^{-/-}$ cell lines. Table S1 shows a comparison of plasma cell tumor incidence in p*Aicda*$^{+/-}$ vs p*Aicda*$^{-/-}$ mice. Table S2 presents summary of FISH data showing proportions of IgH/c-Myc fusion signals in tissue sections. Table S3 shows results of PCR screening of AID-sufficient Bcl-xL-transgenic mice for T(12;15)-translocation positive clones, and Table S4 provides sequences and positions of primers used for the screening. The online version of this article is available at http://www.jem.org/cgi/content/full/jem.20070882/DC1.

We thank Andre Nussenzweig (NCI), J. Frederic Mushinski (NCI), and Herbert C Morse III (National Institute of Allergy and Infectious Disease [NIAID]) for reading the manuscript and making valuable suggestions; Val Bliskovsky (NCI) for sequencing BACs and PCR products; Brad Burkholder (NCI) for genotyping, Rick Dreyfuss (NIH) for photo micrography, and Jianxun Feng (NIAID) for assistance with Southern blotting. We are grateful to Konrad Huppi (NCI) and Makiko Takizawa (NIAMS) for sharing ideas and reagents; and Sabine Mai (Manitoba Institute of Cell Biology) for technical tips.

This work was supported by the Intramural Research Program of the National Institutes of Health (NCI and NIAID).

The authors have no conflicting financial interests.

Submitted: 3 May 2007
Accepted: 17 October 2007

REFERENCES

1. Ohno, S., M. Babonits, F. Wiener, J. Spira, G. Klein, and M. Potter. 1979. Nonrandom chromosome changes involving the Ig gene-carrying chromosomes 12 and 6 in pristane-induced mouse plasmacytomas. *Cell.* 18:1001–1007.
2. Suematsu, S., T. Matsusaka, T. Matsuda, S. Ohno, J.-I. Miyazaki, K.-I. Yamamura, T. Hirano, and T. Kishimoto. 1992. Generation of plasmacytomas with the chromosomal translocation t(12;15) in interleukin 6 transgenic mice. *Proc. Natl. Acad. Sci. USA.* 89:232–235.
3. Kovalchuk, A.L., T. Kishimoto, and S. Janz. 2000. Lymph nodes and Peyer's patches of IL-6 transgenic BALB/c mice harbor T(12;15) translocated plasma cells that contain illegitimate exchanges between the immunoglobulin heavy-chain mu locus and c-myc. *Leukemia.* 14: 1127–1135.
4. Wiener, F., S. Silva, H. Sugiyama, M. Babonits, H. Axelson, P. Chinmay, and G. Klein. 1990. Mouse plasmacytoma associated (MPC) T(15;16) translocation occurs repeatedly in new MPC induction system. *Curr. Top. Microbiol. Immunol.* 166:107–119.
5. Cory, S. 1986. Activation of cellular oncogenes in hemopoietic cells by chromosome translocation. *Adv. Cancer Res.* 47:189–211.
6. Corcoran, L.M., S. Cory, and J.M. Adams. 1985. Transposition of the immunoglobulin heavy chain enhancer to the myc oncogene in a murine plasmacytoma. *Cell.* 40:71–79.
7. Fahrlander, P.D., J. Sumegi, J.-Q. Yang, F. Wiener, K.B. Marcu, and G. Klein. 1985. Activation of the c-myc oncogene by the immunoglobulin heavy-chain gene enhancer after multiple switch region-mediated chromosome rearrangements in a murine plasmacytoma. *Proc. Natl. Acad. Sci. USA.* 82:3746–3750.
8. Shapiro, M.A., and M. Weigert. 1987. A complex translocation at the murine kappa light-chain locus. *Mol. Cell. Biol.* 7:4130–4133.
9. Shaughnessy, J., F. Wiener, K. Huppi, J.F. Mushinski, and M. Potter. 1994. A novel c-myc-activating reciprocal T(12;15) chromosomal

translocation juxtaposes S alpha to Pvt-1 in a mouse plasmacytoma. *Oncogene*. 9:247–253.
10. Ohno, S., S. Migita, and S. Murakami. 1991. c-myc gene in a murine plasmacytoma without visible chromosomal translocations moves to chromosome 12F1 with Pvt-1 and rearranges with IgH enhancer-S mu sequences. *Int. J. Cancer*. 49:102–108.
11. Muramatsu, M., V.S. Sankaranand, S. Anant, M. Sugai, K. Kinoshita, N.O. Davidson, and T. Honjo. 1999. Specific expression of activation-induced cytidine deaminase (AID), a novel member of the RNA-editing deaminase family in germinal center B cells. *J. Biol. Chem*. 274: 18470–18476.
12. Muramatsu, M., K. Kinoshita, S. Fagarasan, S. Yamada, Y. Shinkai, and T. Honjo. 2000. Class switch recombination and hypermutation require activation-induced cytidine deaminase (AID), a potential RNA editing enzyme. *Cell*. 102:553–563.
13. Revy, P., T. Muto, Y. Levy, F. Geissmann, A. Plebani, O. Sanal, N. Catalan, M. Forveille, R. Dufourcq-Labelouse, A. Gennery, et al. 2000. Activation-induced cytidine deaminase (AID) deficiency causes the autosomal recessive form of the Hyper-IgM syndrome (HIGM2). *Cell*. 102:565–575.
14. Petersen-Mahrt, S.K., R.S. Harris, and M.S. Neuberger. 2002. AID mutates *E. coli* suggesting a DNA deamination mechanism for antibody diversification. *Nature*. 418:99–103.
15. Franco, S., F.W. Alt, and J.P. Manis. 2006. Pathways that suppress programmed DNA breaks from progressing to chromosomal breaks and translocations. *DNA Repair (Amst.)*. 5:1030–1041.
16. Lieber, M.R., K. Yu, and S.C. Raghavan. 2006. Roles of nonhomologous DNA end joining, V(D)J recombination, and class switch recombination in chromosomal translocations. *DNA Repair (Amst.)*. 5:1234–1245.
17. Doi, T., K. Kinoshita, M. Ikegawa, M. Muramatsu, and T. Honjo. 2003. De novo protein synthesis is required for the activation-induced cytidine deaminase function in class-switch recombination. *Proc. Natl. Acad. Sci. USA*. 100:2634–2638.
18. Begum, N.A., N. Izumi, M. Nishikori, H. Nagaoka, R. Shinkura, and T. Honjo. 2007. Requirement of non-canonical activity of uracil DNA glycosylase for class switch recombination. *J. Biol. Chem*. 282:731–742.
19. Ramiro, A.R., M. Jankovic, T. Eisenreich, S. Difilippantonio, S. Chen-Kiang, M. Muramatsu, T. Honjo, A. Nussenzweig, and M.C. Nussenzweig. 2004. AID is required for c-myc/IgH chromosome translocations in vivo. *Cell*. 118:431–438.
20. Ramiro, A.R., M.C. Nussenzweig, and A. Nussenzweig. 2006. Switching on chromosomal translocations. *Cancer Res*. 66:7837–7839.
21. Byrd, L.G., A.H. McDonald, L.G. Gold, and M. Potter. 1991. Specific pathogen-free BALB/cAn mice are refractory to plasmacytoma induction by pristane. *J. Immunol*. 147:3632–3637.
22. Fagarasan, S., M. Muramatsu, K. Suzuki, H. Nagaoka, H. Hiai, and T. Honjo. 2002. Critical roles of activation-induced cytidine deaminase in the homeostasis of gut flora. *Science*. 298:1424–1427.
23. Silva, S., A.L. Kovalchuk, J.S. Kim, G. Klein, and S. Janz. 2003. BCL2 accelerates inflammation-induced BALB/c plasmacytomas and promotes novel tumors with coexisting T(12;15) and T(6;15) translocations. *Cancer Res*. 63:8656–8663.
24. Cheung, W.C., J.S. Kim, M. Linden, L. Peng, B. Van Ness, R.D. Polakiewicz, and S. Janz. 2004. Novel targeted deregulation of c-Myc cooperates with Bcl-X(L) to cause plasma cell neoplasms in mice. *J. Clin. Invest*. 113:1763–1773.
25. Strasser, A., A.W. Harris, and S. Cory. 1993. E mu-bcl-2 transgene facilitates spontaneous transformation of early pre-B and immunoglobulin-secreting cells but not T cells. *Oncogene*. 8:1–9.
26. Potter, M. 1984. Genetics of susceptibility to plasmacytoma development in BALB/c mice. *Cancer Surv*. 3:247–264.
27. Anderson, A.O., J.S. Wax, and M. Potter. 1985. Differences in the peritoneal response to pristane in BALB/cAnPt and BALB/cJ mice. *Curr. Top. Microbiol. Immunol*. 122:242–253.
28. Aloisi, F., and R. Pujol-Borrell. 2006. Lymphoid neogenesis in chronic inflammatory diseases. *Nat. Rev. Immunol*. 6:205–217.
29. Drayton, D.L., S. Liao, R.H. Mounzer, and N.H. Ruddle. 2006. Lymphoid organ development: from ontogeny to neogenesis. *Nat. Immunol*. 7:344–353.
30. Hamada, H., T. Hiroi, Y. Nishiyama, H. Takahashi, Y. Masunaga, S. Hachimura, S. Kaminogawa, H. Takahashi-Iwanaga, T. Iwanaga, H. Kiyono, et al. 2002. Identification of multiple isolated lymphoid follicles on the antimesenteric wall of the mouse small intestine. *J. Immunol*. 168:57–64.
31. Potter, M., and F. Wiener. 1992. Plasmacytomagenesis in mice: model of neoplastic development dependent upon chromosomal translocations. *Carcinogenesis*. 13:1681–1697.
32. Muller, J.R., S. Janz, and M. Potter. 1995. Differences between Burkitt's lymphomas and mouse plasmacytomas in the immunoglobulin heavy chain/c-myc recombinations that occur in their chromosomal translocations. *Cancer Res*. 55:5012–5018.
33. Kovalchuk, A.L., E.B. Mushinski, and S. Janz. 2000. Clonal diversification of primary BALB/c plasmacytomas harboring T(12;15) chromosomal translocations. *Leukemia*. 14:909–921.
34. Wiener, F., and M. Potter. 1993. Myc-associated chromosomal translocations and rearrangements in plasmacytomagenesis in mice. In The causes and consequences of chromosomal aberrations. I.R. Kirsch, editor. CRC Press, Inc. Boca Raton, FL.
35. Axelson, H., Y. Wang, S. Silva, M.G. Mattei, and G. Klein. 1994. Juxtaposition of N-myc and Ig kappa through a reciprocal t(6;12) translocation in a mouse plasmacytoma. *Genes Chromosomes Cancer*. 11:85–90.
36. Wang, Y., H. Sugiyama, H. Axelson, C.K. Panda, M. Babonits, A. Ma, J.M. Steinberg, F.W. Alt, G. Klein, and F. Wiener. 1992. Functional homology between N-myc and c-myc in murine plasmacytomagenesis: plasmacytoma development in N-myc transgenic mice. *Oncogene*. 7:1241–1247.
37. Rooney, S., J. Sekiguchi, S. Whitlow, M. Eckersdorff, J.P. Manis, C. Lee, D.O. Ferguson, and F.W. Alt. 2004. Artemis and p53 cooperate to suppress oncogenic N-myc amplification in progenitor B cells. *Proc. Natl. Acad. Sci. USA*. 101:2410–2415.
38. Unniraman, S., S. Zhou, and D.G. Schatz. 2004. Identification of an AID-independent pathway for chromosomal translocations between the Igh switch region and Myc. *Nat. Immunol*. 5:1117–1123.
39. Nacht, M., A. Strasser, Y.R. Chan, A.W. Harris, M. Schlissel, R.T. Bronson, and T. Jacks. 1996. Mutations in the p53 and SCID genes cooperate in tumorigenesis. *Genes Dev*. 10:2055–2066.
40. Vanasse, G.J., J. Halbrook, S. Thomas, A. Burgess, M.F. Hoekstra, C.M. Disteche, and D.M. Willerford. 1999. Genetic pathway to recurrent chromosome translocations in murine lymphoma involves V(D)J recombinase. *J. Clin. Invest*. 103:1669–1675.
41. Zhu, C., K.D. Mills, D.O. Ferguson, C. Lee, J. Manis, J. Fleming, Y. Gao, C.C. Morton, and F.W. Alt. 2002. Unrepaired DNA breaks in p53-deficient cells lead to oncogenic gene amplification subsequent to translocations. *Cell*. 109:811–821.
42. Difilippantonio, M.J., S. Petersen, H.T. Chen, R. Johnson, M. Jasin, R. Kanaar, T. Ried, and A. Nussenzweig. 2002. Evidence for replicative repair of DNA double-strand breaks leading to oncogenic translocation and gene amplification. *J. Exp. Med*. 196:469–480.
43. Celeste, A., S. Difilippantonio, M.J. Difilippantonio, O. Fernandez-Capetillo, D.R. Pilch, O.A. Sedelnikova, M. Eckhaus, T. Ried, W.M. Bonner, and A. Nussenzweig. 2003. H2AX haploinsufficiency modifies genomic stability and tumor susceptibility. *Cell*. 114:371–383.
44. Fernandez-Capetillo, O., A. Lee, M. Nussenzweig, and A. Nussenzweig. 2004. H2AX: the histone guardian of the genome. *DNA Repair (Amst.)*. 3:959–967.
45. Ward, I.M., S. Difilippantonio, K. Minn, M.D. Mueller, J.R. Molina, X. Yu, C.S. Frisk, T. Ried, A. Nussenzweig, and J. Chen. 2005. 53BP1 cooperates with p53 and functions as a haploinsufficient tumor suppressor in mice. *Mol. Cell. Biol*. 25:10079–10086.
46. Ramiro, A.R., M. Jankovic, E. Callen, S. Difilippantonio, H.T. Chen, K.M. McBride, T.R. Eisenreich, J. Chen, R.A. Dickins, S.W. Lowe, et al. 2006. Role of genomic instability and p53 in AID-induced c-myc-Igh translocations. *Nature*. 440:105–109.
47. Difilippantonio, M.J., J. Zhu, H.T. Chen, E. Meffre, M.C. Nussenzweig, E.E. Max, T. Ried, and A. Nussenzweig. 2000. DNA repair protein Ku80 suppresses chromosomal aberrations and malignant transformation. *Nature*. 404:510–514.

48. Bassing, C.H., H. Suh, D.O. Ferguson, K.F. Chua, J. Manis, M. Eckersdorff, M. Gleason, R. Bronson, C. Lee, and F.W. Alt. 2003. Histone H2AX: a dosage-dependent suppressor of oncogenic translocations and tumors. *Cell*. 114:359–370.
49. Woo, Y., S.M. Wright, S.A. Maas, T.L. Alley, L.B. Caddle, S. Kamdar, J. Affourtit, O. Foreman, E.C. Akeson, D. Shaffer, et al. 2007. The nonhomologous end joining factor Artemis suppresses multi-tissue tumor formation and prevents loss of heterozygosity. *Oncogene*. 26: 6010–6020.
50. Roth, D.B., T.N. Porter, and J.H. Wilson. 1985. Mechanisms of nonhomologous recombination in mammalian cells. *Mol. Cell. Biol.* 5:2599–2607.
51. Roth, D.B. 2002. Amplifying mechanisms of lymphomagenesis. *Mol. Cell*. 10:1–2.
52. Weitzman, S.A., A.B. Weitberg, E.P. Clark, and T.P. Stossel. 1985. Phagocytes as carcinogens: malignant transformation produced by human neutrophils. *Science*. 227:1231–1233.
53. Barzilai, A., and K. Yamamoto. 2004. DNA damage responses to oxidative stress. *DNA Repair (Amst.)*. 3:1109–1115.
54. Shacter, E., E.J. Beecham, J.M. Covey, K.W. Kohn, and M. Potter. 1988. Activated neutrophils induce prolonged DNA damage in neighboring cells. *Carcinogenesis*. 9:2297–2304.
55. Shacter, E., R.L. Lopez, E.J. Beecham, and S. Janz. 1990. DNA damage induced by phorbol ester-stimulated neutrophils is augmented by extracellular cofactors. *J. Biol. Chem*. 265:6693–6699.
56. Valko, M., M. Izakovic, M. Mazur, C.J. Rhodes, and J. Telser. 2004. Role of oxygen radicals in DNA damage and cancer incidence. *Mol. Cell. Biochem*. 266:37–56.
57. Tanaka, T., H.D. Halicka, X. Huang, F. Traganos, and Z. Darzynkiewicz. 2006. Constitutive histone H2AX phosphorylation and ATM activation, the reporters of DNA damage by endogenous oxidants. *Cell Cycle*. 5:1940–1945.
58. Vilenchik, M.M., and A.G. Knudson. 2003. Endogenous DNA double-strand breaks: production, fidelity of repair, and induction of cancer. *Proc. Natl. Acad. Sci. USA*. 100:12871–12876.
59. Fang, W., D.L. Mueller, C.A. Pennell, J.J. Rivard, Y.S. Li, R.R. Hardy, M.S. Schlissel, and T.W. Behrens. 1996. Frequent aberrant immunoglobulin gene rearrangements in pro-B cells revealed by a bcl-xL transgene. *Immunity*. 4:291–299.
60. Fang, W., B.C. Weintraub, B. Dunlap, P. Garside, K.A. Pape, M.K. Jenkins, C.C. Goodnow, D.L. Mueller, and T.W. Behrens. 1998. Self-reactive B lymphocytes overexpressing Bcl-xL escape negative selection and are tolerized by clonal anergy and receptor editing. *Immunity*. 9:35–45.
61. Alves, N.L., R.A. van Lier, and E. Eldering. 2007. Withdrawal symptoms on display: Bcl-2 members under investigation. *Trends Immunol*. 28:26–32.
62. Giono, L.E., and J.J. Manfredi. 2006. The p53 tumor suppressor participates in multiple cell cycle checkpoints. *J. Cell. Physiol*. 209:13–20.
63. Livingstone, L.R., A. White, J. Sprouse, E. Livanos, T. Jacks, and T.D. Tlsty. 1992. Altered cell cycle arrest and gene amplification potential accompany loss of wild-type p53. *Cell*. 70:923–935.
64. Yin, Y., M.A. Tainsky, F.Z. Bischoff, L.C. Strong, and G.M. Wahl. 1992. Wild-type p53 restores cell cycle control and inhibits gene amplification in cells with mutant p53 alleles. *Cell*. 70:937–948.
65. Askew, D.S., R.A. Ashmun, B.C. Simmons, and J.L. Cleveland. 1991. Constitutive c-myc expression in an IL-3-dependent myeloid cell line suppresses cell cycle arrest and accelerates apoptosis. *Oncogene*. 6: 1915–1922.
66. Evan, G.I., A.H. Wyllie, C.S. Gilbert, T.D. Littlewood, H. Land, M. Brooks, C.M. Waters, L.Z. Penn, and D.C. Hancock. 1992. Induction of apoptosis in fibroblasts by c-myc protein. *Cell*. 69:119–128.
67. Grillot, D.A., R. Merino, J.C. Pena, W.C. Fanslow, F.D. Finkelman, C.B. Thompson, and G. Nunez. 1996. *bcl-x* exhibits regulated expression during B cell development and activation and modulates lymphocyte survival in transgenic mice. *J. Exp. Med*. 183:381–391.
68. Boise, L.H., M. Gonzalez-Garcia, C.E. Postema, L. Ding, T. Lindsten, L.A. Turka, X. Mao, G. Nunez, and C.B. Thompson. 1993. bcl-x, a bcl-2-related gene that functions as a dominant regulator of apoptotic cell death. *Cell*. 74:597–608.
69. Liyanage, M., A. Coleman, S. du Manoir, T. Veldman, S. McCormack, R.B. Dickson, C. Barlow, A. Wynshaw-Boris, S. Janz, J. Wienberg, et al. 1996. Multicolour spectral karyotyping of mouse chromosomes. *Nat. Genet*. 14:312–315.
70. Chu, C.C., W.E. Paul, and E.E. Max. 1992. Quantitation of immunoglobulin mu-gamma 1 heavy chain switch region recombination by a digestion-circularization polymerase chain reaction method. *Proc. Natl. Acad. Sci. USA*. 89:6978–6982.